Surface polishing and modification of Ti-6Al-4V alloy by shear thickening polishing

Jiahuan Wang[1,2,4], Yu Zhou[1,2], Zhen Qiao[3], Saurav Goel[4,5], Jinhu Wang[1,2], Xu Wang[1,2], Hongyu Chen[1,2], Julong Yuan[1,2] and Binghai Lyu[1,2*]

[1] College of Mechanical Engineering, Zhejiang University of Technology, Hangzhou, 310023, China

[2] Ultra-precision Machining Center, Key Laboratory of Special Purpose Equipment and Advanced Manufacturing Technology, Zhejiang University of Technology, Hangzhou, 310023, China

[3] General Practice Department, Third people's Hospital of Hangzhou, Hangzhou, 310009, China

[4] School of Engineering, London South Bank University, London, SE1 0AA, UK

[5] Department of Mechanical Engineering, University of Petroleum and Energy Studies, Dehradun, 248007, India

Abstract:

In this study, a comparison of three newly developed polishing techniques namely, shear thickening polishing (STP), Chemistry enhanced STP (C-STP) and Electrolysis enhanced STP (E-STP) was made to investigate their suitability to Ti-6Al-4V biomaterials polishing and modification, which can produce Beilby layer after polishing and enhance mechanical and biological performance. The surface roughness S_a after STP was about 13.8 nm with a material removal rate of 54.3 nm/min. The C-STP showed the lowest surface roughness of 7.2 nm which was almost half that of STP and the MRR during C-STP was almost 2.1 times that of the conventional STP. The STP did not lead to any change of the surface composition, whereas a 136 nm thick Beilby layer was observed to form during the C-STP which revealed a lower friction coefficient of 0.04 as well as improved osteoblast cell activity. The E-STP showed an intermittent improvement as it provided a surface roughness of 10.2 nm and 1.6 times MRR than that obtained from conventional STP. Due to the dense oxide film of about 60 nm, the E-STP processed surface showed the best wettability and corrosion resistance. Overall, we reveal an important pathway for achieving scalable finishing on Ti-6Al-4V with desirable surface characteristics.

Keywords:

Ti-6Al-4V alloy; shear thickening polishing; surface modification; surface characteristics; biomaterials

Abbreviations:

STP: Shear thickening polishing
C-STP: Chemistry enhanced shear thickening polishing
E-STP: Electrolysis enhanced shear thickening polishing
MRR: Material removal rate
UVA: Ultraviolet radiation A, ultraviolet radiation with wavelengths between 320 and 400 nm
a-C coating: Amorphous carbon coating
CMP: Chemical mechanical polishing

AFF: Abrasive flow finishing
b-TNTZ alloy: beta Titanium-Niobium-Tantalum-Zirconium alloy
XPS: X-ray photoelectron spectroscopy
DMEM: Dulbecco’s modified eagle’s medium
FBS: Fetal bovine serum
PBS: Phosphate buffer saline
MTT: 3-(4,5-Dimethylthiazol-2-yl)-2,5-diphenyltetrazolium bromide
DMSO: Dimethyl sulfoxide
SEM: Scanning electron microscope
ALP: Alkaline phosphates
FIB: Focused ion beam

1. Introduction

Titanium and its alloy play an essential role in biomedical implants due to their excellent mechanical properties, corrosion resistance and biocompatibility [1-4]. These materials are frequently used in implants such as joint replacement, fixed dental implants, set screws, and surgical instruments [5-7].

To improve the service performance and security of titanium implants, different surface treatment methods have been developed to introduce a functional layer of the titanium surface which include methods such as magnetron sputtering [8], plasma spraying [9, 10], ultraviolet irradiation [11], sol-gel [12, 13], chemical vapor deposition [14, 15], laser nitriding [16] and anodization [17].

Beline et al. [8] utilised magnetron sputtering to produce a thin β-Ta_2O_5 film on the cp-Ti surface, which demonstrated long-term stability and favourable biological properties. Zhang et al. [10] investigated the induction suspension plasma spraying technology and a TiO_2 coating was deposited on pure Ti substrates. The results showed that the bionic micro/nanostructured films significantly improved cell adhesion. Lee et al. [11] found that the titanium surface after UVA irradiation has better hydrophilicity due to the production of bone-like apatite film. Cho et al. [15] performed a plasma enhanced chemical vapor deposition method and deposited the amorphous carbon coatings on Ti-6Al-4V alloy. Their results showed that the a-C coating deposited at the bias power of 30 W demonstrates the highest biocompatibility. Chen et al. [18] suggested surface modification through anodic oxidation. The treated surface showed microfine structures and included Ca and P elements, improving cell adhesion behaviour.

The surface topography has been thought to play an important role in the service life of an implant as this comes directly in contact with the body tissue allowing the passage of fluid media as well as cell proliferation and tissue healing [19]. Various surface processing methods are used to finish curved surfaces of titanium implants for delicate applications such as medical implants. For example, manual finishing showed a modicum of success but the efficiency and repeatability are poor [20]. Ozdemir et al. [21] utilised CMP technology to replace traditional etching and sand-blasting. The research found that cell growth was observed to be affected more by the surface roughness. Larsson et al. [22] developed electropolishing of titanium implants and studied the influence of surface roughness on cell activity. Prakash et al. [23] found that processing the b-TNTZ alloy through magneto-rheological polishing effectively reduces the wear of polished knee and acetabular implants and potentially extends their service life. Okada et al. [24] proposed a novel large-area electron beam irradiation to improve surface finish of titanium alloys. Sarkar et al. [25]

employed the AFF technology, compared to the original tool finishing, which could save more than 70% time for the processing knee joint.

All in all, surface treatments are essential for implants with complex shapes. So, a general question we attempt to answer through this paper is whether we can fabricate an implant surface to leave a beneficial functional layer during its surface finishing?

The STP technology utilises shear thickening effect of the non-Newtonian fluid, which is a high efficiency, surface quality and low cost polishing method [26-27]. Shao et al. [29] investigated the STP process of high-temperature nickel-base alloy turbine blades and found that the lowest surface roughness could be obtained at the pH value of 6.5. Span et al. [30] proposed a novel finish machining process in which the medium can adapt to the sharp workpiece. Its non-Newtonian polishing slurry could apply to complex surface sharps finishing and the edge preparation of cutting tools such as drills and end mills. Wang et al. [31] performed C-STP on Ti-6Al-4V alloy and obtained a surface roughness below 10 nm at the pH value of 2. Moreover, the process showed tuneable features as the surface reaction layer with different compositions was obtained.

This study demonstrates the use of STP and its variants such as C-STP and E-STP to report the performance improvement in the surface characteristics of Ti-6Al-4V. These techniques were assessed in terms of the output value of surface roughness, MRR, thickness of Beilby layer, chemical composition, nanomechanical properties, wettability, corrosion resistance, and cell proliferation.

2. Mechanism of different STP processes

The schematic illustration of the STP process is depicted in Fig.1. The slurry during STP flows over the surface of the workpiece which is influenced by the applied shear stress in the contact area. When the shear rate exceeds a threshold value, an effect known as shear thickening occurs. The solid particles dispersed in the slurry aggregate into clusters, causing the abrasive to be surrounded by these solid particles. This rapidly increases the viscosity of the slurry in the contact area, forming a “flexible fixed abrasive tool”. The force applied to the abrasives accelerates the removal of material [26].

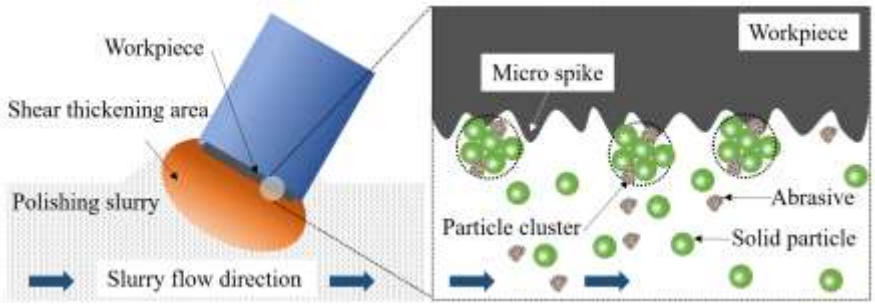

Fig.1 Schematic illustration of the STP

The schematic illustration of the C-STP process is depicted in Fig.2 wherein the chemical agent was added to the polishing slurry of the conventional STP which produces a Beilby layer (the metallurgically transformed layer on the surface left after polishing) on the surface of the polished surface of the workpiece [32]. With the synergy of chemical and mechanical removal modes, this process yields higher quality and efficiency than the conventional STP. In the case of Ti-6Al-4V, the C-STP process leaves behind a residual Beilby layer, the effects of which were investigated in this work.

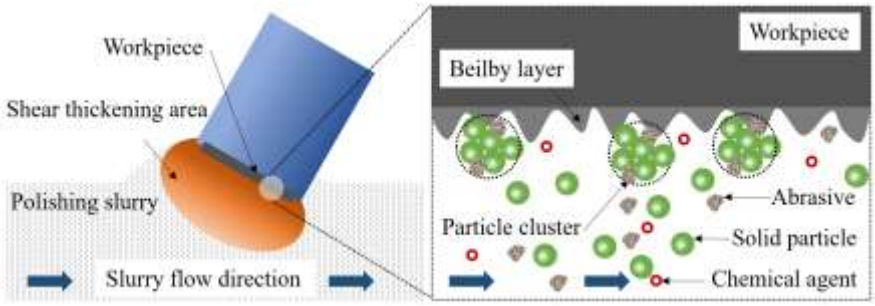

Fig.2 Schematic illustration of the C-STP

The schematic illustration of the E-STP process is shown in Fig.3 wherein beside adding a chemically active electrolyte, a potential difference is applied to harness the combined influence of electrolytic and shear thickening effects. Here the workpiece serves as the anode, and the graphite plate on the bottom of the polishing tank serves as the cathode. Under the action of anodic oxidation, an oxide film forms on the surface and the mechanical action removes it. Similar to C-STP, this process leaves behind a Beilby layer on the polished surface.

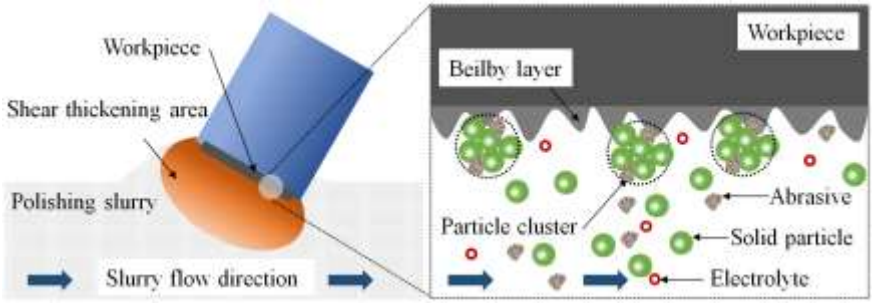

Fig.3 Schematic of the E-STP

3. Experimental methodology

3.1 Sample preparation

This study utlised flat workpieces of Ti-6Al-4V with a size of Ø25.4×2 mm for the polishing experiments. The results also provide a reference to compare the polishing performance on the curved Ti-6Al-4V surfaces. The composition of the Ti-6Al-4V titanium alloy (TC4, XINSHENG METAL Material Co. LTD, China) is shown in Table 1. Prior to polishing, the sample was rubbed manually with a 1000 # sandpaper to remove foreign particles, oxide layers and bring evenness in the sample. This caused the Ti-6Al-4V workpiece to have a starting surface roughness of about 100±10 nm before the polishing experiments.

Table 1 Chemical composition of the Ti-6Al-4V titanium alloy

Elements	Al	V	Fe	C	N	O	H	Ti
Concentration (wt.%)	6.5	4.22	0.12	0.03	0.01	0.14	0.002	Balance

The study explored three different methods (STP, C-STP and E-STP) to investigate the polishing performance of Ti-6Al-4V samples using the processing parameters shown in Table 2, except for the chemical characteristics of polishing slurry and electrolytic parameters, all other parameters are constant and selected based on previous studies [26, 27, 31, 33].

The slurry composition is crucial to the performance of the STP process. In this case, it was noted that the slurry composition does vary with individual variants of STP in obtaining the optimal

process. In this work, we compared the most optimal combinations of the slurry composition to have an ideal comparison among the three processes, STP, C-STP and E-STP. The slurry preparation starts from the basic abrasive solution which was prepared by adding the colloidal silica (8040, YZ-lapping material, China) into the deionized water. The pH value in the case of conventional STP, C-STP were maintained as 7 and 2 respectively. In the case of E-STP, 3 wt. % KPO_3 was added to configure the E-STP slurry. The multi-hydroxyl powder as solid particle was added into the corresponding abrasive solution and then the mixture was mixed for about 5 min to obtain the final polishing slurry.

Table 2 Experimental parameters

Polishing method	STP	C-STP	E-STP
Chemistry of polishing slurry	pH 7	pH 2	3 wt.% KPO_3
Electrolytic power parameters	-	-	10 V, 0.7 A
Abrasive	colloidal silica	colloidal silica	colloidal silica
Average abrasive size (nm)	80	80	80
Abrasive concentration (wt.%)	10	10	10
Polishing speed (m/s)	2	2	2
Rotation speed of samples (rpm)	10	10	10
Polishing time (min)	15	15	15

The surface polishing experimental setup used to process Ti-6Al-4V samples is shown in Fig.4. During the polishing process, the polishing slurry was filled in the polishing tank and the workpiece was held rigidly in place by a fixture while immersing it into the polishing slurry. The polishing tank and polishing fixture were both rotated to ensure that the workpiece gets polished uniformly. The samples with different processing methods were processed in the corresponding polishing slurry for 15 mins, respectively. The samples polished with E-STP were supplied an extra power with the voltage of 10 V and current of 0.7 A.

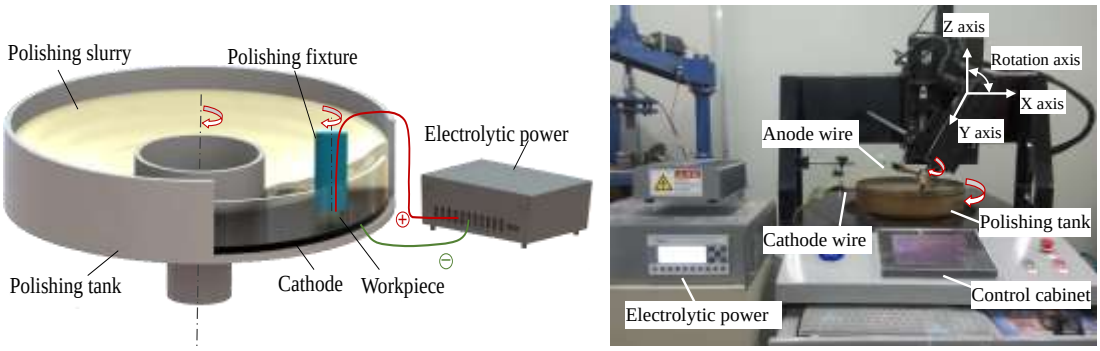

(a) (b)

Fig.4 (a) Schematic of STP, (b) Polishing device employed in this study

3.2 Polishing performance characterization

Surface topography and MRR are critical technical indicators to characterize the machining performance. A precision electronic analytical balance (ME225S, Sartorius, Germany) was used to

measure the weight loss of the sample before and after the polishing. An average of three times polishing data was used to estimate and report the MRR. The 3D surface topography of the Ti-6Al-4V was measured using an optical 3D surface profiler (SuperView W1, Chotest, China) with a 10× interference objective for an area of 489.5×489.5 μm. More than three points were selected randomly to measure the surface topography, and the surface roughness (S_a) was obtained accordingly. The surface microscope images were captured using a depth-of-field microscope (VHX-7000, Keyence, Japan) with a 500× objective.

3.3 Beilby layer thickness and chemical composition estimates

To detect the thickness and composition of the Beilby layer, the samples of Ti-6Al-4V polished with STP variants were cleaned with deionized water and dried. The samples were stored in a vacuum kettle and transferred to the vacuum chamber of the corresponding instrument. X-ray Photoelectron Spectroscopy (ESCALAB 250Xi, Thermo, USA) was performed to investigate the surface state. CasaXPS software was used to analyse and process the spectral data of Ti (2p), Al (2p), P (2p), O (1s), and C (1s) and all peaks were corrected with C(1s) at bonding energy of 284.8 eV. A FIB-SEM (Helios G5 CX, Thermo, USA) was performed to observe the thickness of the Beilby layer. A crater with a size of 30×5 μm was cut by a high current (30 nA) ion beam, and the crater wall was trimmed by a low current (20 pA) ion beam to view the subsurface structure clearly.

3.4 Beilby layer nanomechanical properties test using a nanoindentation

The nano scratch experiment was divided into three stages: in pre-scratch scan, a vertical load of 2 μN was applied on the sample to check surface roughness and tangent slope [34]. In scratch scan, the test was conducted with a ramp load mode in which the peak value was 30 mN, the scratch length was kept constant at 500 μm and the scratch velocity was 50 μm/s. In post-scratch scan, a vertical load of 2 μN was applied to scan the scribing marks and analyze the elastic recovery of the material after loading. Scratch spacing was above 20 μm to avoid overlapping of deformation areas caused by the adjacent scratches. At least three scratch tests were performed under the same test conditions to ensure repeatability.

3.5 Surface wettability measurements

The contact angle of the polished surface was measured by a contact angle measuring instrument (OCA35, Dataphysics, Germany). Hank’s solution was used to mimic body fluid environment. The droplet size of each experiment was strictly controlled to be 5 μL through a microtiter, and the experiments were performed for 3 times at least. The droplet’s contact angle was calculated with the analysis software provided by the instrument.

3.6 Corrosion resistance measurements

The corrosion resistance of the samples polished with different methods in Hank’s solution was tested using an electrochemical workstation (760e, CH Instruments, China). A three-electrode electrolytic cell was used. The platinum electrode with a size of 20×20×0.2 mm was used as the counter electrode and the Ag/AgCl electrode filled with saturated potassium chloride solution was

used as the reference electrode. Finally, the sample was used as working electrode with a working/exposed area of 1 cm^2. The open circuit potential test was first checked. If the change of the open circuit potential in 3 mins was less than 5 mV then the working electrode was considered to be in the stable state. Also, the potentiodynamic polarisation plots were tested with a scanning rate of 5 mV/s and a scanning voltage range from -1 to 1 V (relative to the reference electrode).

3.7 Biological studies

3.7.1 Osteoblastic cell culture

The osteoblast cells (MC3T3-E1, ATCC, USA) were cultured in high glucose Dulbecco’s modified eagle medium (DMEM, Gbico, USA) containing 10% fetal bovine serum (FBS, Gbico, USA) in a 37°C incubator (Thermo Forma, Thermo, USA) while the concentration of CO_2 was 5% and the relative humidity was 90%. The culture medium was changed every two days, the cells were washed with PBS to get rid of metabolic waste. The culture cells were separated into four groups and treated with samples processed with STP, C-STP, E-STP method and Petri dishes (control group).

3.7.2 MTT assay

MC3T3-E1 cells at the logarithmic growth stage were diluted to a density of 1×10^5 cells/ml and inoculated on the samples of four different groups. The DMEM was added and placed in the incubator overnight. After the cells adhered to the wall, the growth medium was removed and replaced by DMEM containing 3-(4,5-Dimethylthiazol-2-yl)-2,5-diphenyltetrazolium bromide (MTT, Beyotime Biotechnology, China), and then continued to grow in the incubator for 3 hours. Finally, the supernatant was removed and 1 ml of DMSO was added to dissolve the precipitate until it became homogeneous. The absorbance value was measured at 490 nm using an optical absorption microplate reader (SPECTRAmax190, Molecular Devices, USA), and each group of experiments was performed at least three times.

3.7.3 SEM observation

After the cells were grown for 24 hours and washed 3 times using PBS and fixed with glutaraldehyde, they were dehydrated in alcohol step by step and dried in a desiccator. The samples were sprayed with gold and placed in the SEM vacuum chamber for observation.

3.7.4 ALP assay

All the culture medium was soaked after the cells grew for 3 days and 6 days, and it was washed twice with PBS and processed with 0.25% trypsin for 1 min. Cell precipitation was obtained after centrifuging. 500 μL TritonX-100 with a concentration of 1% was added, which was blown repeatedly and cleaved for 40 min. The absorbance value was detected at 405 nm wavelength by an optical absorption microplate reader. The experiment was repeated three times to ensure the reliability of the results.

4. Results and discussions

4.1 Material removal rate and surface topography of Ti-6Al-4V during STP

The results obtained for surface roughness and MRR of Ti-6Al-4V samples polished with traditional STP, C-STP and E-STP are shown in Fig.5. The STP process provided a surface roughness S_a of 13.8 ± 0.8 nm at an MRR of 54.3 nm/min. C-STP as opposed to other STP methods showed the lowest surface roughness S_a of 7.2 ± 1.0 nm and the highest MRR of 118.0 nm/min. The E-STP process resulted in a surface roughness S_a of 10.2 ± 0.7 nm at an MRR of 89.5 nm/min. These results indicated that both chemical etching and electrochemical oxidation improve the polishing performance compared to conventional STP. The typical microscope images of Ti-6Al-4V alloy surface polished with different methods are shown in Fig.6 (a-1) (b-1) (c-1). A key observation was that the polished surface obtained from E-STP showed a yellowish layer formed as a result of the electrolytic oxidation.

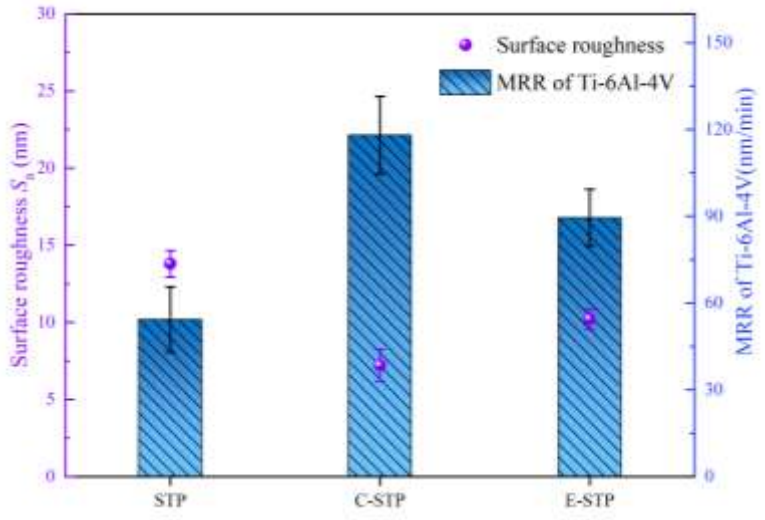

Fig.5 Surface roughness and MRR of Ti-6Al-4V polished with different methods

The typical 3D surface topography of Ti-6Al-4V surface polished with different methods are shown in Fig.6 (a-2) (b-2) (c-2). The observation revealed that all the surface topography obtained from conventional STP, C-STP and E-STP are nanometrically smooth which surface roughness is sub 15 nm. As shown in Fig.6 (a-2), many spikes were observed on the surface after STP. They were caused by the uneven removal of different alloy phases due to the single mechanical action. As shown in Fig.6 (b-2), the polished surface was significantly smoother after C-STP than STP. According to the pH-potential diagram of the titanium-water system [35], it is known that titanium corrodes easily under acidic conditions. However, titanium can also easily be passivated and it forms an oxide film under neutral or alkaline conditions [31, 36]. Therefore, with the assistance of acid polishing slurry, lower surface roughness and higher MRR can be obtained by C-STP due to the excellent synergy between mechanical mode of removal and chemical etching. As shown in Fig.6 (c-2), the surface polished with E-STP showed prominent bumps and the propensity of defects was much larger than STP. According to the literature, the oxide film on the Ti-6Al-4V surface due to the electrolysis downgrades the surface roughness [37].

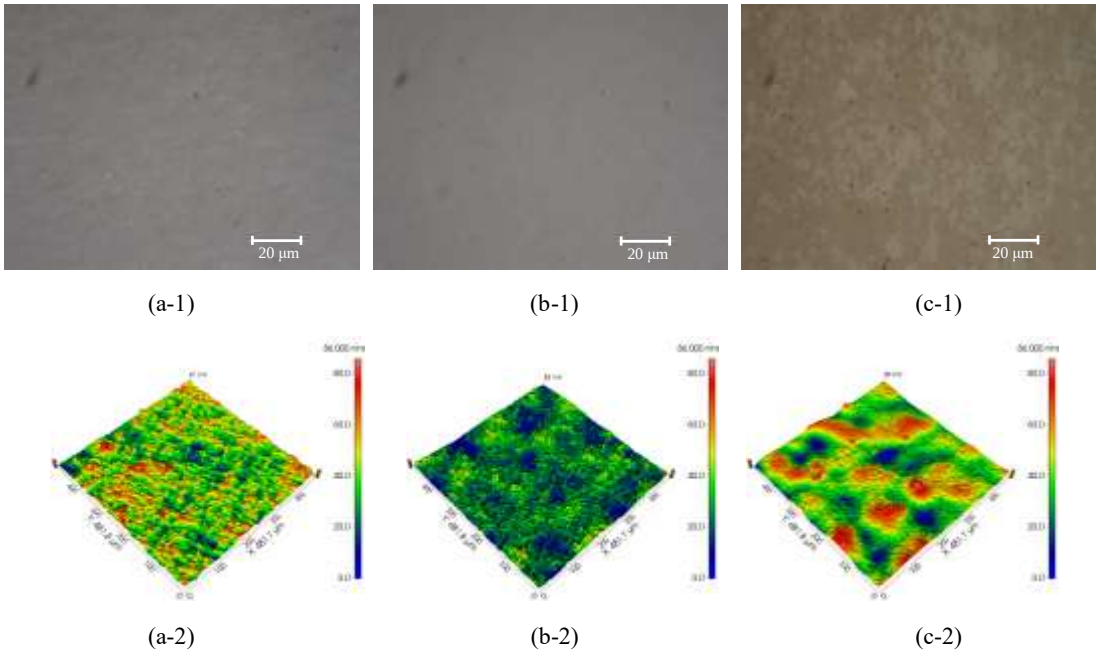

Fig.6: Typical surface topography of Ti-6Al-4V polished with different methods. (a-1) microscopic image after STP, (b-1) microscopic image after C-STP, (c-1) microscopic image after E-STP; (a-2) 3D topography after STP, S_a 13.5nm, (b-2) 3D topography after C-STP, S_a 7.0 nm, (c-2) 3D topography after E-STP, S_a 10.8 nm.

4.2 Analysis of the chemical composition of the Beilby layer

Fig.7 shows the thickness of the Beilby layer observed on the polished surface whilst using different polishing methods. No Beilby layer was found after STP processing, as the material was removed purely by the mechanical action of abrasive particles. A surface Beilby layer with a thickness of 136 nm was observed on surface after C-STP processing. The thickness of the surface Beilby layer after E-STP processing was about 60 nm thick.

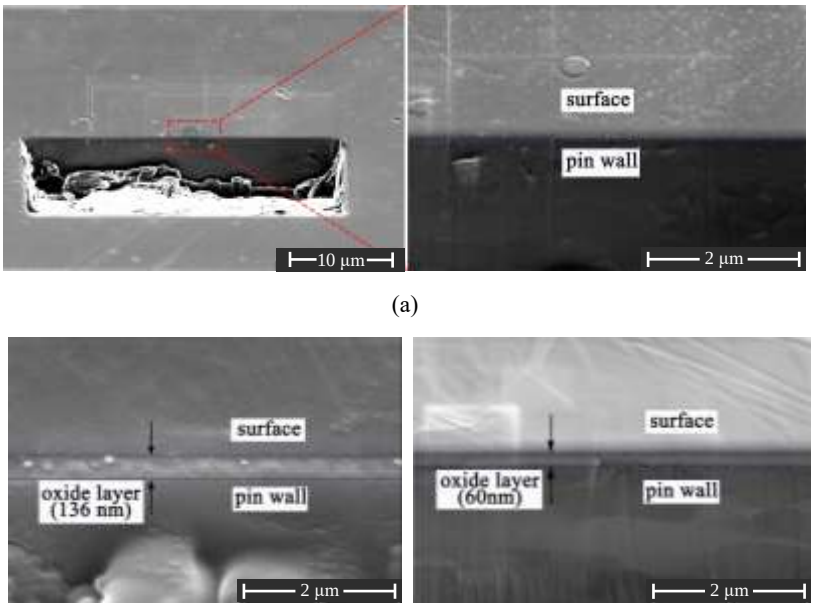

Fig.7 Observation of the surface Beilby layer after polished with different metods through FIB-SEM (a) sample polished by STP, (b) C-STP, (c) E-STP.

The Beilby layer formed on the Ti-6Al-4V surface polished with C-STP was thicker than E-STP. This can be ascribed to a slower chemical reaction rate, allowing for deeper penetration of the chemicals into the workpiece surface during C-STP. Contrarily, the rate of electrochemical reactions in case of E-STP was higher, leading to the generation of a denser oxide film on the electrolyzed surface which prevents further oxidation reaction. This results in a slower MRR during E-STP compared to C-STP.

To accurately identify the composition of Beilby layer, XPS analysis was performed (see Fig.8). The corresponding Ti(2p) spectrum is presented in Fig.8 (a), the deconvolution of Ti-6Al-4V surface processed with STP and C-STP show four peaks [36]. The main peak with the highest binding energy of 458.8 eV correspond to Ti^{4+}, the peak with a binding energy of 456.8 eV correspond to Ti^{3+}, and the peak with a binding energy of 454.6 eV correspond to Ti^{2+} and the peak with the lowest binding energy of 483.3 eV correspond to Ti. Nevertheless, the surface polished with E-STP only showed one peak corresponding to Ti^{4+}. These results indicated strong oxidisation during the electrolysis process which transforms the metallic Ti to Ti^{4+}. The high valence state of Ti on the surface polished with STP or C-STP can be attributed to the action of oxygen in the air or polishing slurry [38].

The O(1s) spectrum revealed two peaks [39] shown in Fig.8 (b). The peak with higher binding energy of 532.0 eV referred to OH^- and the peak with lower binding energy was assigned to O^{2-}. The P(2p) spectrum is shown in Fig.8 (c) and the deconvolution of sample polished with C-STP showed significant peaks at the binding energy of 133.6 eV. Based on the literature, this peak seems to refer to the formation of PO_4^{3-} [40-41].

As shown in Fig.8 (d), the Al(2p) spectrum processed with STP and C-STP revealed two peaks [42-43]. These were the peak with higher binding energy of 74 eV which can be assigned to Al^{3+} and the other peak with binding energy of 71.3 eV can be assigned to Al. Moreover, the samples processed with E-STP showed just one peak with binding energy of 74 eV, which corresponds to Al^{3+}.

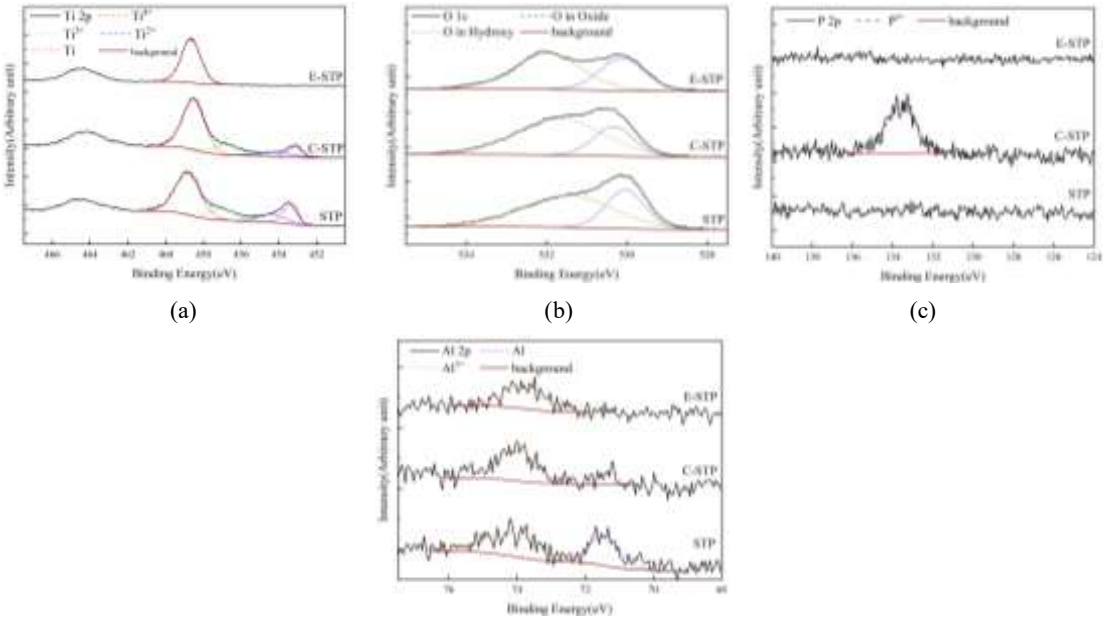

(a) (b) (c)

(d)

Fig.8: XPS spectra of Ti-6Al-4V surface polished with different methods, (a) Ti (2p) spectrum, (b) O (1s) spectrum, (c) P (2p) spectrum, (d) Al (2p) spectrum.

The percentage of Ti^{4+}, Ti^{3+}, Ti^{2+}, Ti, Al^{3+} and Al on the surface of the sample presented in Table 3, were calculated based on the relative area of elements in different chemical valence states. It is obvious that the Ti-6Al-4V surface polished with E-STP contained no metallic Ti or Al. However, some residual metallic Ti and Al was present on the surface polished with C-STP and STP. Due to the chemical etching effect of acidic polishing slurry, less metal Ti and Al remain on the surface polished with C-STP than STP.

Table 3 The percentage of Ti^{4+}, Ti^{3+}, Ti^{2+}, Ti, Al^{3+} and Al on the surface after polishing with different methods.

Process method	Ti^{4+}	Ti^{3+}	Ti^{2+}	Ti	Al^{3+}	Al
STP	56.0	17.9	12.0	14.1	57.6	42.4
C-STP	66.9	16.6	8.6	7.8	86.3	13.7
E-STP	100	-	-	-	100	-

According to previous research [44,45], although the STP involves solely mechanical removal by abrasive particles, titanium and aluminum are highly reactive metals that can react with oxygen in the polishing slurry or air. Additionally, the resulting film on titanium alloys usually with a thickness of 5-6 nm [46], makes it difficult to observe through FIB-SEM techniques. The resulting reaction formulas can be described as below:

$$2Ti + O_2 \rightarrow 2TiO \quad (1)$$

$$4TiO + O_2 \rightarrow 2Ti_2O_3 \quad (2)$$

$$2Ti_2O_3 + O_2 \rightarrow 4TiO_2 \quad (3)$$

$$Al + O_2 \rightarrow Al_2O_3 \quad (4)$$

As indicated above, during the C-STP, phosphoric acid and oxygen react with Ti [47] or Al and phosphoric acid compounds were generated.

$$Ti + H_3PO_4 \rightarrow TiPO_4 + H_2 \quad (5)$$

$$TiPO_4 + H_3PO_4 + O_2 \rightarrow Ti_3(PO_4)_4 + H_2O \quad (6)$$

$$Al + H_3PO_4 \rightarrow AlPO_4 + H_2 \quad (7)$$

The electrolytic oxidation during the E-STP is an ‘intense’ process, which is distinct from the ‘gentle’ chemical reaction during C-STP and the instant formation of dense oxide film of TiO_2 [48] and Al_2O_3 covers the surface. The main reaction formula during the E-STP can be inferred as:

$$Ti + 2H_2O \rightarrow TiO_2 + H_2 \quad (8)$$

$$Al + H_2O \rightarrow Al_2O_3 + H_2 \quad (9)$$

4.3 Friction properties measurement through wear tests

The plot of lateral fore versus normal force obtained from scratching on Ti-6Al-4V surface polished with different methods are shown in Fig. 9 (a) and the friction coefficient results are shown in Fig. 9 (b). The surface polished with C-STP showed the least lateral force during scratching with its least coefficient of friction as ~0.04. The surface polished with E-STP showed a friction coefficient of about 0.16. These differences can be ascribed to the presence of Beilby layer left on the surface of C-STP polished surfaces which lowers the friction values. Fig. 9 (c) shows the assessment of friction coefficient and the corresponding SEM images obtained from the nano-scratch tests on all polished surfaces (STP, C-STP and E-STP). The surface polished with STP showed evidence of plastic deformation while the surface polished with C-STP and E-STP showed elastic deformation mechanism. What’s more, the Beilby layer of the surface polished with E-STP was thinner than that of C-STP, which resulted in cracking along the trace on both sides of the center,

particularly in high load areas.

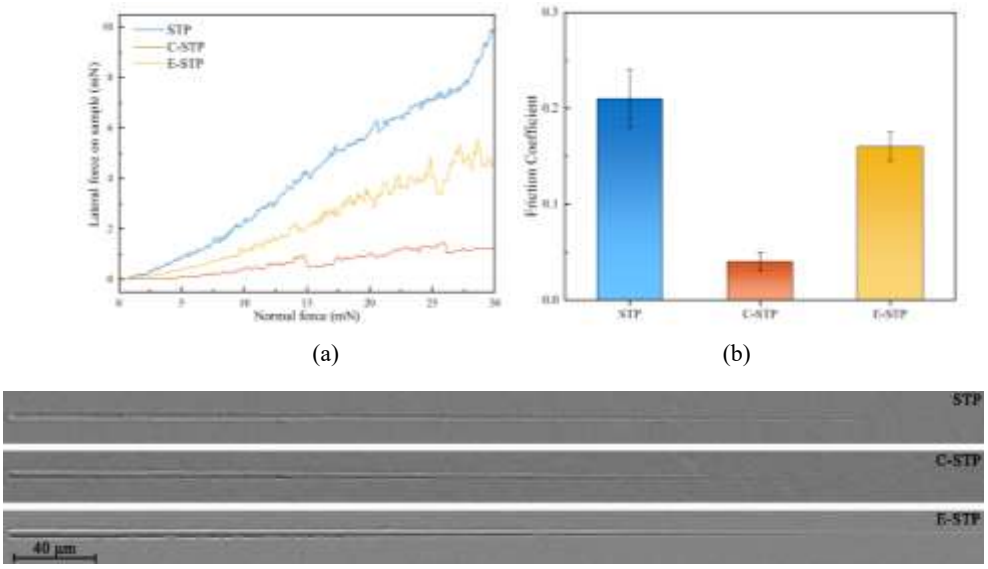

Fig. 9 (a) Typical lateral force versus normal force curves of Ti-6Al-4V surface polished with different methods, (b) Coefficient of friction for all polished surfaces, (c) corresponding wear tracks seen through the SEM

4.4 Wettability assessment

The surface wettability of titanium implants is directly related to the adsorption of cells as well as proteins. Implants with high hydrophilicity can significantly enhance bone growth [51]. As shown in Fig.10, the contact angles of surface polished with STP, C-STP and E-STP are measured to be 65.0°, 68.7° and 59.6°, respectively. It points to the difference in the surface energy of the machined metallurgical layer left on the surface after polishing. The high surface polarity of TiO_2 results in easy binding with water molecules [52], leading to the best wettability for the surface polished with E-STP process. As for the surface processed with C-STP, a smoother surface structure led to the observation of the largest contact angle [53].

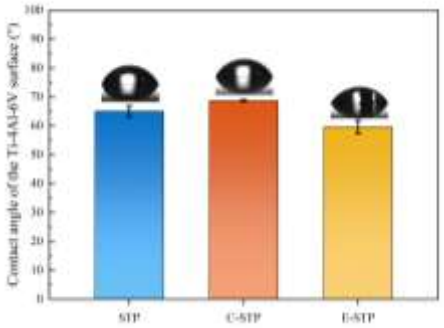

Fig.10 Wettability tests results of Ti-6Al-4V surface polished with different methods.

4.5 Corrosion resistance

Biocorrosion of Ti alloys when used as an implant is a common occurrence and this process results in the release of metal ions [54] which can be detrimental to the health. This section investigated the corrosion resistance of Ti-6Al-4V surface polished with different methods in Hank’s solution using a potentiodynamic polarization test. The results from the corrosion tests are shown

in Fig.11. It can be seen from the polarisation curves that the anodic processes of samples polished with E-STP are strongly suppressed compared to that of STP and C-STP. The corrosion potential E_{corr} and corrosion current density I_{corr} obtained through Tafel analysis are presented in Table 4. The E_{corr} of surface polished with STP, C-STP, and E-STP increases in that order, while the I_{corr} decreases in that order. It can be concluded that the surface processed with E-STP possessed the best corrosion resistance in Hank’s solution, which was attributed to the denser oxide film on the polished surface. The Beilby layer of C-STP processed sample improved the corrosion resistance to some extent, but the improvement was limited.

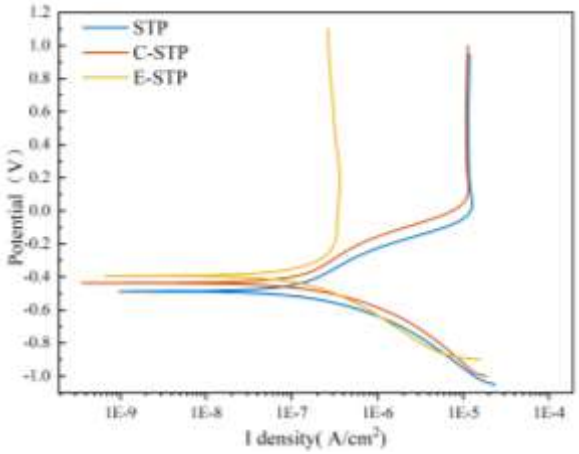

Fig.11 The potentiodynamic polarisation plots of the surface polished with different methods in the Hank’s solution.

Table 4 Corrosion potential E_{corr} and corrosion current density I_{corr} by the Tafel analysis.

Preparing method	E_{coor} (V)	I_{coor}(A/cm^2)
STP	-0.481	1.344×10^{-7}
C-STP	-0.438	1.139×10^{-7}
E-STP	-0.392	8.588×10^{-8}

4.6 Cell culture

Ti-6Al-4V surface as an implant requires osseointegration for strong attachment with the bone to support its growth [55]. To investigate this aspect, MC3T3-E1 cells as immortalized cell lines were derived from mouse skull tissue [56]. Those were cultured on the three types of polished Ti-6Al-4V surfaces for a day. The SEM images of MC3T3-E1 cell morphology observed after a day of culture on various types of polished surfaces are shown in Fig.12. It can be seen that the MC3T3-E1 cells on all three samples showed good growth with filamentous and lamellipodium extensions. These features indicate strong adhesion to all types of Ti-6Al-4V polished surfaces.

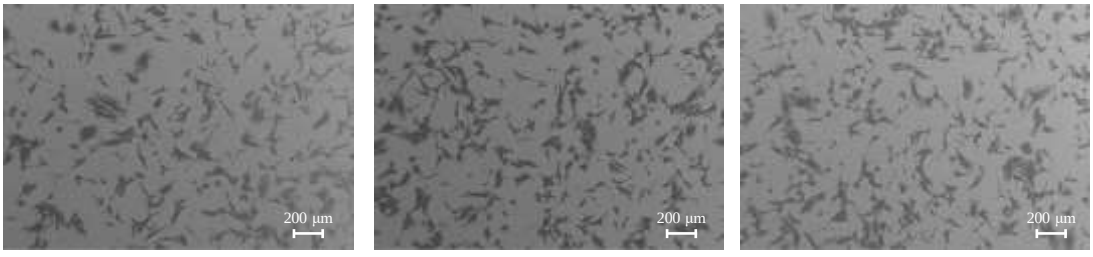

(a) (b) (c)

Fig.12 SEM images of MC3T3-E1 cell morphology cultured for 1 day on Ti-6Al-4V surface polished with different methods (a) STP, (b) C-STP, (c) E-STP.

The MTT assay was performed to evaluate cell proliferation in vitro by reducing succinate dehydrogenase in the mitochondria of living cells to blue-purple methylzan [57]. As shown in Fig.13 (a), there was no significant difference in the proliferation capacity of the surface polished with STP, C-STP and E-STP methods compared to the control group.

ALP activity is an important marker of the early stage of osteoblast differentiation [58]. Fig.13(b) shows MC3T3-E1 cell activity tested by ALP assay after 3 and 6 days of incubation on Ti-6Al-4V surface polished with different methods. In all cases, the ALP activity increased over time regardless of the polishing method employed. However, the C-STP polished sample showed exceptional ALP growth activity, while the surface polished with STP or E-STP methods showed similarity with the control group. Prior research indicates that inorganic phosphate enhances bone formation [18, 58-60] and this would mean that the Beilby layer formed after C-STP enhanced the ALP activity.

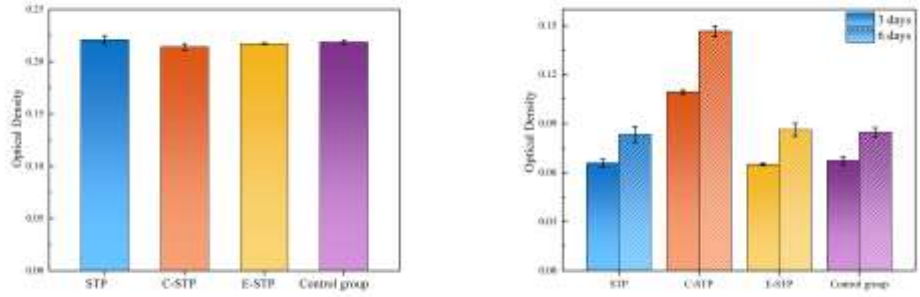

(a) (b)

Fig.13 (a) MC3T3-E1 cell viability tested by MTT assay after 3 days of incubation on Ti-6Al-4V surface polished with different methods (b) MC3T3-E1 cell activity tested by ALP assay after 3 and 6 days of incubation on surface polished with different methods

5 Conclusion

The paper provides novel insights into the mechanics of material removal and biological functionality of Ti-6Al-4V surfaces processed by three newly emerging polishing techniques namely, STP, C-STP and E-STP. These polishing methods in general were found very suitable for scalable polishing of finished biomedical implants, however, the influence of Beilby layer (the metallurgically transformed layer on the surface left after polishing) was found to differ significantly in all cases resulting in a marked influence on the surface properties and biological functionality in all cases. The overall conclusions from this study can be summarized as below:

The conventional STP technique performed on Ti-6Al-4V surface revealed a roughness S_a of about 13.8 nm at an optimal MRR of 54.3 nm/min. The C-STP process reduced the roughness further down to S_a 7.2 nm while enhancing the MRR by 2.1 times than that of the conventional STP. The E-STP process showed an intermittent improvement as it provided a surface roughness S_a of 10.2 nm and 1.6 times MRR than that obtained from conventional STP. Overall all three methods were competitive to finish polish Ti-6Al-4V surface to near about 10 nm finishing. This was well inline with the relevant ASTM standard that suggests the surface roughness (R_a) on the metallic knee joint implants to be lower than 100 nm [61].

The conventional STP process did not affect the finished metallurgical layer on the polished surface as much as the C-STP surface. During C-STP, the Beilby layer of about 136 nm thickness

comprising of a metal phosphate was observed to form on the surface. In the case of E-STP, a different type of surface composition layer with a thickness of 60 nm and composition of TiO_2 and Al_2O_3 was observed to form.

The C-STP finished Ti-6Al-4V alloy showed lower coefficient of friction and higher osteoblast activity compared to the other two methods. On the other hand, the E-STP polished surface showed better wettability and corrosion resistance.

Overall, those three newly polishing method shows new hopes in the arena of finish machining and polishing Ti-6Al-4V surfaces. This could for instance be applied onto the 3D printed titanium implants which have very high roughness after printing and needs finished polishing with techniques proposed and assessed in this paper.

Acknowledgement:

This paper received financial support in form of National Natural Science Foundation of China (52175441), Natural Science Foundation of Zhejiang Provincial (LD22E050010), National Natural Science Foundation of China (52175442) and a travel scholarship from the China Scholarship Council (CSC Grant No. 202208330333) to station at LSBU labs to work closely with Prof Goel.

SG would like to acknowledge the funding support from UKRI via Grants No. EP/S036180/1 and EP/T024607/1, feasibility study awards to LSBU from the UKRI National Interdisciplinary Circular Economy Hub (EP/V029746/1) and Transforming the Foundation Industries: a Network+ (EP/V026402/1).

Reference

[1] Liu C, Goel S, Llavori I, et al. Benchmarking of several material constitutive models for tribology, wear, and other mechanical deformation simulations of Ti-6Al-4V. Journal of the mechanical behavior of biomedical materials, 2019, 97: 126-137.

[2] Larrañaga-Altuna M, Zabala A, Llavori I, et al. Bactericidal surfaces: An emerging 21st-century ultra-precision manufacturing and materials puzzle. Applied Physics Reviews, 2021, 8(2): 021303.

[3] Montañez N D, Carreño H, Escobar P, et al. Functional evaluation and testing of a newly developed Teleost’s Fish Otolith derived biocomposite coating for healthcare. Scientific reports, 2020, 10(1): 258.

[4] Wang K, Wang L, Zheng K, et al. High-efficiency forming processes for complex thin-walled titanium alloys components: State-of-the-art and perspectives. International Journal of Extreme Manufacturing, 2020, 2(3): 032001.

[5] Dargusch M S, Sivarupan T, Bermingham M, et al. Challenges in laser-assisted milling of titanium alloys. International Journal of Extreme Manufacturing, 2020, 3(1): 015001.

[6] Kirthika S K, Goel G, Matthews A, et al. Review of the untapped potentials of antimicrobial materials in the construction sector. Progress in Materials Science, 2022: 101065.

[7] Patel N R, Gohil P P. A review on biomaterials: scope, applications & human anatomy significance. International Journal of Emerging Technology and Advanced Engineering, 2012, 2(4): 91-101.

[8] Beline T, de Almeida A B, Neto N F A, et al. β-Ta2O5 thin film for implant surface modification triggers superior anti-corrosion performance and cytocompatibility of titanium. Applied Surface Science, 2020, 520: 146326.

[9] Ong J L, Carnes D L, Bessho K. Evaluation of titanium plasma-sprayed and plasma-sprayed hydroxyapatite implants in vivo. Biomaterials, 2004, 25(19): 4601-4606.

[10] Zhang W, Gu J, Zhang C, et al. Preparation of titania coating by induction suspension plasma spraying for biomedical application. Surface and Coatings Technology, 2019, 358: 511-520.

[11] Lee T C, Abdullah H Z, Koshy P, et al. Ultraviolet-assisted biomimetic coating of bone-like apatite on anodized titanium for biomedical applications. Thin Solid Films, 2018, 660: 191-198.

[12] Domínguez-Trujillo C, Peón E, Chicardi E, et al. Sol-gel deposition of hydroxyapatite coatings on porous titanium for biomedical applications. Surface and Coatings Technology, 2018, 333: 158-162.

[13] Kim H W, Koh Y H, Li L H, et al. Hydroxyapatite coating on titanium substrate with titania buffer layer processed by sol–gel method. Biomaterials, 2004, 25(13): 2533-2538.

[14] da Cruz N C, Rangel E C, Wang J, et al. Properties of titanium oxide films obtained by PECVD. Surface and Coatings Technology, 2000, 126(2-3): 123-130.

[15] Cho Y S, Liao L K, Hsu C H, et al. effect of substrate bias on biocompatibility of amorphous carbon coatings deposited on Ti-6Al-4V by PECVD. Surface and Coatings Technology, 2019, 357: 212-217.

[16] Chan C W, Lee S, Smith G, et al. Enhancement of wear and corrosion resistance of beta titanium alloy by laser gas alloying with nitrogen. Applied Surface Science, 2016, 367: 80-90.

[17] Vilardell A M, Cinca N, Garcia-Giralt N, et al. In-vitro study of hierarchical structures: Anodic oxidation and alkaline treatments onto highly rough titanium cold gas spray coatings for biomedical applications. Materials Science and Engineering: C, 2018, 91: 589-596.

[18] Chen C S, Tsao Y L, Wang D J, et al. Research on cell behavior related to anodized and hydrothermally treated titanium surface. Applied surface science, 2013, 271: 1-6.

[19] Rompen E, Domken O, Degidi M, et al. The effect of material characteristics, of surface topography and of implant components and connections on soft tissue integration: a literature review. Clinical oral implants research, 2006, 17: 55.

[20] Barman A, Das M. Nano-finishing of bio-titanium alloy to generate different surface morphologies by changing magneto-rheological polishing fluid compositions. Precision Engineering, 2018, 51: 145-152.

[21] Ozdemir Z, Ozdemir A, Basim G B. Application of chemical mechanical polishing process on titanium based implants. Materials Science and Engineering: C, 2016, 68: 383-396.

[22] Larsson C, Thomsen P, Aronsson B O, et al. Bone response to surface-modified titanium implants: studies on the early tissue response to machined and electropolished implants with different oxide thicknesses. Biomaterials, 1996, 17(6): 605-616.

[23] Prakash C, Singh S, Pramanik A, et al. Experimental investigation into nano-finishing of β-TNTZ alloy using magneto-rheological fluid magnetic abrasive finishing process for orthopedic applications. Journal of Materials Research and Technology, 2021, 11: 600-617.

[24] Okada A, Uno Y, Yabushita N, et al. High efficient surface finishing of bio-titanium alloy by large-area electron beam irradiation. Journal of Materials Processing Technology, 2004, 149(1-3): 506-511.

[25] Sarkar M, Jain V K. Nanofinishing of freeform surfaces using abrasive flow finishing process. Proceedings of the Institution of Mechanical Engineers, Part B: Journal of Engineering Manufacture, 2017, 231(9): 1501-1515.

[26] Li M, Lyu B, Yuan J, et al. Shear-thickening polishing method. International Journal of machine tools and manufacture, 2015, 94: 88-99.

[27] Li M, Lyu B, Yuan J, et al. Evolution and equivalent control law of surface roughness in shear-thickening polishing. International Journal of Machine Tools and Manufacture, 2016, 108: 113-126.

[28] Guo L, Wang X, Lyu B, et al. Shear-thickening Polishing of inner raceway surface of bearing and suppression of edge effect. The International Journal of Advanced Manufacturing Technology, 2022, 121(5-6): 4055-4068.

[29] Shao Q, Lyu B, Yuan J, et al. Shear thickening polishing of the concave surface of high-temperature nickel-based alloy turbine blade. Journal of Materials Research and Technology, 2021, 11: 72-84.

[30] Chan J, Koshy P. Tool edge honing using shear jamming abrasive media. CIRP Annals, 2020, 69(1): 289-292.

[31] Wang J, Lyu B, Jiang L, et al. Chemistry enhanced shear thickening polishing of Ti–6Al–4V. Precision Engineering, 2021, 72: 59-68

[32] Katiyar N K, Goel G, Hawi S, et al. Nature-inspired materials: Emerging trends and prospects. NPG Asia Materials, 2021, 13(1): 56.

[33] Chen C, Chen J, Chao C, et al. Electrochemical characteristics of surface of titanium formed by electrolytic polishing and anodizing. Journal of materials science, 2005, 40: 4053-4059.

[34] Faisal N H, Ahmed R, Goel S, et al. Influence of test methodology and probe geometry on nanoscale fatigue failure of diamond-like carbon film. Surface and coatings technology, 2014, 242: 42-53.

[35] Muñoz-Portero M J, García-Antón J, Guiñón J L, et al. Pourbaix diagrams for titanium in concentrated aqueous lithium bromide solutions at 25° C. Corrosion science, 2011, 53(4): 1440-1450.

[36] Deng C, Jiang L, Qin N, et al. Effects of pH and H2O2 on the chemical mechanical polishing of titanium alloys. Journal of Materials Processing Technology, 2021, 295: 117204.

[37] Jáquez-Muñoz J M, Gaona-Tiburcio C, Chacón-Nava J, et al. Electrochemical corrosion of titanium and titanium alloys anodized in H2SO4 and H3PO4 solutions. Coatings, 2022, 12(3): 325.

[38] Liang C, Liu W, Li S, et al. A nano-scale mirror-like surface of Ti–6Al–4V attained by chemical mechanical polishing. Chinese Physics B, 2016, 25(5): 058301.

[39] Ferguson J D, Weimer A W, George S M. Atomic layer deposition of ultrathin and conformal Al2O3 films on BN particles. Thin Solid Films, 2000, 371(1-2): 95-104.

[40] Bui T H, Hong S P, Yoon J. Development of nanoscale zirconium molybdate embedded anion exchange resin for selective removal of phosphate. Water research, 2018, 134: 22-31.

[41] Wang Z, Kong D, Wang M, et al. Sealing effect of surface porosity of Ti–P composite films on tinplates. RSC advances, 2019, 9(23): 12990-12997.

[42] Jeon I Y, Shin S H, Choi H J, et al. Heavily aluminated graphene nanoplatelets as an efficient flame-retardant. Carbon, 2017, 116: 77-83.

[43] Lee P M, Liu Y S, Villamagua L, et al. Experimental observation and computer simulation of Al/Sn substitution in p-type aluminum nitride-doped tin oxide thin film. The Journal of Physical Chemistry C, 2016, 120(8): 4211-4218.

[44] N. Cabrera, N. Mott, Theory of the oxidation of metals, Rep. Prog. Phys. 12 (1949) 163–184.

[45] Trzciński W A, Cudziło S, Paszula J. Studies of free field and confined explosions of aluminium enriched RDX compositions. Propellants, Explosives, Pyrotechnics: An International Journal Dealing with Scientific and Technological Aspects of Energetic Materials, 2007, 32(6): 502-508.

[46] Pantaroto H N, Cordeiro J M, Pereira L T, et al. Sputtered crystalline TiO2 film drives improved surface properties of titanium-based biomedical implants. Materials Science and Engineering: C, 2021, 119: 111638.

[47] Straumanis M E, Chen P C. The corrosion of titanium in acids—the rate of dissolution in sulfuric, hydrochloric, hydrobromic and hydroiodic acids. Corrosion, 1951, 7(7): 229-237.

[48] Li X, Xue Y, Dehoff R, et al. Hierarchically-Structured Ti/TiO2 Electrode for Hydrogen Evolution Synthesized via 3D Printing and Anodization. Journal of Energy and Power Technology, 2020, 2(2).

[49] Yu Y, Xu X Q, Zhang T, et al. Investigation on the microstructural and mechanical properties of a Polytetrafluoroethylene thin film by radio frequency magnetron sputtering. Thin Solid Films, 2020, 712: 138302.

[50] Huang L, Xu K, Lu J, et al. Nano-scratch and fretting wear study of DLC coatings for biomedical application. Diamond and related materials, 2001, 10(8): 1448-1456.

[51] Aliasghari S, Skeldon P, Thompson G E. Plasma electrolytic oxidation of titanium in a phosphate/silicate electrolyte and tribological performance of the coatings. Applied Surface Science, 2014, 316: 463-476.

[52] Li Y, Wang W, Yu F, et al. Characterization and cytocompatibility of hierarchical porous TiO2 coatings incorporated with calcium and strontium by one-step micro-arc oxidation. Materials Science and Engineering: C, 2020, 109: 110610.

[53] Burton Z, Bhushan B. Hydrophobicity, adhesion, and friction properties of nanopatterned polymers and scale dependence for micro-and nanoelectromechanical systems. Nano letters, 2005, 5(8): 1607-1613.

[54] Delgado-Ruiz R, Romanos G. Potential causes of titanium particle and ion release in implant dentistry: a systematic review. International journal of molecular sciences, 2018, 19(11): 3585.

[55] Zhang F, Hu Q, Wei Y, et al. Surface modification of Titanium implants by pH-Responsive coating designed for Self-Adaptive antibacterial and promoted osseointegration. Chemical Engineering Journal, 2022, 435: 134802.

[56] Kodama H, Amagai Y, Sudo H, et al. Establishment of a clonal osteogenic cell line from newborn mouse calvaria. Japanese Journal of Oral Biology, 1981, 23(4): 899-901.

[57] Li J, Li T T, Zhang Y, et al. A two-step strategy to deposit a hydroxyapatite coating on polydopamine-coated polymer fibers. Biomedical Materials, 2022, 18(1): 015025.

[58] Jeong J, Kim J H, Shim J H, et al. Bioactive calcium phosphate materials and applications in bone regeneration. Biomaterials research, 2019, 23(1): 1-11.

[59] Ito A, Otsuka M, Kawamura H, et al. Zinc-containing tricalcium phosphate and related materials for promoting bone formation. Current Applied Physics, 2005, 5(5): 402-406.

[60] Chang Y L, Stanford C M, Keller J C. Calcium and phosphate supplementation promotes bone cell mineralization: Implications for hydroxyapatite (HA)‐enhanced bone formation. Journal of Biomedical Materials Research: An Official Journal of The Society for Biomaterials, The Japanese Society for Biomaterials, and The Australian Society for Biomaterials and the Korean Society for Biomaterials, 2000, 52(2): 270-278.

[61] Sidpara A M, Jain V K. Nanofinishing of freeform surfaces of prosthetic knee joint implant. Proceedings of the Institution of Mechanical Engineers, Part B: Journal of Engineering Manufacture, 2012, 226(11): 1833-1846.